Available online at www.sciencedirect.com

ScienceDirect

Comput. Methods Appl. Mech. Engrg. 196 (2006) 118–133

Computer methods in applied mechanics and engineering

www.elsevier.com/locate/cma

Prediction of crack evolution and effective elastic behavior of damage-tolerant brittle composites ☆

H.K. Lee [a,*], S. Šimunović [b]

[a] *Department of Civil and Environmental Engineering, Korea Advanced Institute of Science and Technology, Guseong-dong, Yuseong-gu, Daejon 305-701, South Korea*

[b] *Computer Science and Mathematics Division, Oak Ridge National Laboratory, Oak Ridge, TN 37831-6164, United States*

Received 17 June 2005; received in revised form 25 October 2005; accepted 17 February 2006

Abstract

A constitutive model based on a combination of a fracture-mechanics based model and micromechanical formulations is developed to predict the crack evolution and effective mechanical behavior of damage-tolerant brittle composites. The constitutive model is cast in a rate form and considers microcrack nucleation rate and microcrack growth rate. The effective moduli of the composites containing different crack distributions are formulated using the self-consistent method and differential scheme. The constitutive model is then implemented into finite element codes to solve boundary value problems of the composites. Numerical simulations on a benchmark problem are carried out to illustrate the model features. Finally, to further assess the validity of the present framework, the present predictions are compared with experimental data on brittle composites.
Published by Elsevier B.V.

Keywords: Fracture-mechanics based model; Nucleation and growth of microcracks; Degradation of stiffness; Randomly distributed cracks and aligned cracks; Experimental comparison

1. Introduction

Microcrack nucleation, growth and coalescence are the main mechanisms for degradation of effective elastic properties of damage-tolerant brittle materials under monotonously increasing external loads [30]. It has been reported that the crack nucleation is dominant during the early stages of load application [2], followed by the growth of nucleated cracks, and the crack growth eventually results in coalescence of cracks [39]. These processes in general do not possess a recurring kinematic character that could be exploited for unification of the theory over a wide range of loading types and magnitudes.

Explicit modeling of the details of evolving damage and microstructure is still restricted to fundamental studies of material [35,18,6,43,27]. The statistical aspects of failure of brittle materials, size effects, and fundamental description of damage as a multi-scale phenomena have been an increasingly active area of research during the last decade [14,17,9,37,7,42,12].

In damage-tolerant brittle materials, the crack stress field enhancement is countered by the crack shielding, which in some circumstances grants us precious increments of extrapolation of the mean field theories into the area of material

☆ The submitted manuscript has been authored by a contractor of the US Government under contract No. DE-AC05-00OR22725. Accordingly, the US Government retains a nonexclusive, royalty-free license to publish or reproduce the published form of this contribution, or allow others to do so, for US Government purposes.

* Corresponding author. Tel.: +82 42 869 3623.
E-mail address: leeh@kaist.ac.kr (H.K. Lee).

0045-7825/$ - see front matter Published by Elsevier B.V.
doi:10.1016/j.cma.2006.02.008

softening [24,49,21,22]. This indicates our intent to apply the mean field model to the modeling of material failure. In doing so, we are aware of the numerous limitations that have been challenged so many times in the past (see, e.g., [26,4,40,39,16,23,19,38]). However, the physics of the problem that we are interested in allows us to use such mean-field model excursions to a moderate extent. The modeling of this final stage within continuum mechanics framework involves theoretical and mathematical difficulties that so far have evaded unified theoretical and practical solutions.

A fracture-mechanics based constitutive model incorporating micromechanical formulations is developed in the present study for modeling of crack evolution and effective mechanical behavior of damage-tolerant brittle composites. The novelty in the present derivation is its rate form and the flexibility to represent a wide range of stress–strain curves with limited number of model parameters. Moreover, the proposed model is capable of representing the softening effect that is a signature macroscopic characteristic of damage localization. The model is applicable for the situations in which softening occurs by uncorrelated growth of cracks. It is also possible to extend the proposed model to be used within a cohesive band framework [4] to account for localization of damage, or alternatively the discretization of a domain has to be such that the finite element size corresponds to the characteristic size of failure localization features.

The following sections describe the model development and its implementation into finite element (FE) codes. The FE numerical procedures for solving the system of equations constituting the material model have shown to be very important for the numerical efficiency and stability of the model. Numerical simulations are carried out to illustrate key features of the developed model. Finally, the prediction based on the developed model is compared with experimental data to assess the validity of the present framework.

2. A fracture-mechanics based constitutive model for brittle composites

2.1. Overview

Let us start by considering a damage-tolerant brittle composite. We assume that the damaged state can be described by the number of microcracks per unit volume N and the average size of microcracks $\bar{c}$. It is obvious that the microcracks in the real composites will not be straight nor penny-shaped, and their size and orientation distributions will vary from specimen to specimen. However, our premise is that their cumulative effect on the effective material properties can be qualitatively and quantitatively described by using simple approximation of the evolving microstructural disorder $(N, \bar{c})$.

The two damage processes, crack nucleation and crack growth, are assumed to occur sequentially and independently. The rationale for this assumption, besides the obvious motivation for a simplification of the problem, has roots in physics and theory of damage evolution in damage tolerant materials. The process of microcrack nucleation is related to the distribution of the weak sites in the material [14,7,29]. In the heterogeneous materials, the process is stochastic and the microcracks initiate uniformly across the material volume [17]. This allows us to model the nucleation process using a scalar field that implies uncorrelated crack position and orientation. As the weak spots are depleted with the increasing load, the microcracks start to grow. A shift of dominance from nucleation to crack growth is most likely gradual, and therefore our approach can be portrayed as the first approximation to this transition. In the present derivation, the microcrack orientation distribution is assumed to be uniform and the size distribution is assumed to be exponential. These assumptions are more restrictive for the crack growth regime and can be eliminated by considering oriented systems of cracks.

In the present study, a microcrack nucleation model employing Seaman et al.'s [45] exponential rate equation is followed by the application of the formulation of crack growth based on model by Addessio and Johnson [1]. Damage surfaces that define regions of crack growth are based on the volume averaging procedures that implicitly assume absence of crack interaction. The appealing characteristic of this damage surface model is the minimal number of model parameters with respect to the complexity of the process that it is describing. The simplicity commonly translates into robustness of numerical algorithms when modeling complex problems.

The rate of crack growth is assumed to be a function of overstress, i.e., the distance in the stress space between the current stress and the damage surface. For stress states that exceed the current damage threshold, cracks grow. The effective moduli of brittle composites containing different crack distributions will be formulated using the self-consistent method and differential scheme in Section 3. The details of the rate constitutive equations and rates of nucleation and growth of microcracks are presented in the following sections.

2.2. Rate constitutive equations

The constitutive relation for a brittle composite with microcracks distributed in a statistically uniform manner can be expressed as

$$\boldsymbol{\sigma} = \mathbf{C}(N, \bar{c}) : \boldsymbol{\epsilon}, \tag{1}$$

where ":" denotes the tensor contraction, $\boldsymbol{\sigma}$ is the macroscopic stress, $\mathbf{C}$ is the overall stiffness tensor and $\boldsymbol{\epsilon}$ is the macroscopic strain. It is assumed that the damage is proportional. Accordingly, the rate form of Eq. (1) can be proposed in additive form as

$$\dot{\boldsymbol{\sigma}} = \frac{\partial \mathbf{C}}{\partial N}\dot{N} : \boldsymbol{\epsilon} + \frac{\partial \mathbf{C}}{\partial \bar{c}}\dot{\bar{c}} : \boldsymbol{\epsilon} + \mathbf{C} : \dot{\boldsymbol{\epsilon}}. \tag{2}$$

The material model is therefore defined by microcrack nucleation rate $\dot{N}$, microcrack growth rate $\dot{\bar{c}}$, and their respective effect on the overall stiffness tensor.

A numerical integration algorithm needs to be employed to integrate the rate equation in Eq. (2). Let us assume that t_n ($n = 1, 2, 3, \ldots, N$) denotes the time at the end of the nth time step. We seek to determine the unknown state of a local point at the end of the time step with the known results from the previous step. Since the calculation is repeated on a set of procedures, an algorithm that focuses only on a single time step from $t = t_n$ to $t = t_{n+1}$ can be constructed. The increment of total strain $\Delta\boldsymbol{\epsilon}_{n+1}$ is either given or can be obtained from the given strain history. Thus, we have:

$$\boldsymbol{\epsilon}_{n+1} = \boldsymbol{\epsilon}_n + \Delta\boldsymbol{\epsilon}_{n+1}. \tag{3}$$

The following equations are available from the discretization

$$t_{n+1} = t_n + \Delta t_{n+1}, \tag{4}$$
$$\bar{c}_{n+1} = \bar{c}_n + \Delta\bar{c}_{n+1}, \tag{5}$$
$$N_{n+1} = N_n + \Delta N_{n+1}. \tag{6}$$

Consequently, the overall (macroscopic) stress $\boldsymbol{\sigma}_{n+1}$ can be calculated as

$$\boldsymbol{\sigma}_{n+1} = \boldsymbol{\sigma}_n + \mathbf{C} : \Delta\boldsymbol{\epsilon}_{n+1} + \frac{\partial \mathbf{C}}{\partial \bar{c}}\Delta\bar{c}_{n+1} : \boldsymbol{\epsilon}_n + \frac{\partial \mathbf{C}}{\partial \bar{c}}\Delta\bar{c}_{n+1} : \Delta\boldsymbol{\epsilon}_{n+1} + \frac{\partial \mathbf{C}}{\partial N}\Delta N_{n+1} : \boldsymbol{\epsilon}_n + \frac{\partial \mathbf{C}}{\partial N}\Delta N_{n+1} : \Delta\boldsymbol{\epsilon}_{n+1}. \tag{7}$$

Further, the incremental stresses, the incremental pressure, the pressure, and the deviatoric stresses can be obtained from the following relations.

$$\Delta\boldsymbol{\sigma}_{n+1} = \mathbf{C}_{n+1} : \Delta\boldsymbol{\epsilon}_{n+1}, \tag{8}$$
$$\Delta p_{n+1} = -\frac{1}{3}(\Delta\sigma_{11} + \Delta\sigma_{22} + \Delta\sigma_{33})_{n+1}, \tag{9}$$
$$p_{n+1} = p_n + \Delta p_{n+1}, \tag{10}$$
$$\mathbf{q}_{n+1} = \mathbf{q}_n + (\Delta\boldsymbol{\sigma}_{n+1} + \Delta p_{n+1}\delta_{ij}), \tag{11}$$

where δ_{ij} denotes the Kronecker delta and the overall stiffness tensor $\mathbf{C}$ will be defined in Section 3.

2.3. Rate of microcrack nucleation

Through investigations of several materials [3,44,46,8], it has been shown that the nucleation rate of microcracks $\dot{N}$ can be expressed as exponential relations and satisfies the following relation [45]

$$\begin{aligned} \dot{N} &= \dot{N}_0 \cdot \exp\left[\frac{\sigma - \sigma_{n0}}{\sigma_1}\right], \quad \sigma > \sigma_{n0}, \\ &= 0, \quad \sigma < \sigma_{n0}, \end{aligned} \tag{12}$$

where $\dot{N}_0$ and σ_1 denote experimentally determined material parameters, and σ_{n0} signifies the threshold stress for the nucleation of microcracks.

According to the backward Euler method, the following approximation is made for the rate equation for crack nucleation:

$$N_{n+1} = N_n + \Delta t_{n+1}\dot{N}_0 \cdot \exp\left[\frac{(\sigma)_{n+1} - \sigma_{n0}}{\sigma_1}\right]. \tag{13}$$

Consequently, N_{n+1} can be evaluated by defining a scalar nonlinear equation $f(N_{n+1})$ at time $t = t_{n+1}$:

$$f(N_{n+1}) = N_{n+1} - N_n - \Delta t_{n+1}\dot{N}_0 \cdot \exp\left[\frac{(\sigma)_{n+1} - \sigma_{n0}}{\sigma_1}\right]. \tag{14}$$

The root of this equation can be solved by a number of numerical methods. It is noted that the first derivative of Eq. (14) with respect to N_{n+1} can be calculated analytically by exact derivation or numerically by finite difference approximation, providing the tangent for the methods of Newton or Quasi-Newton iteration.

2.4. Rate of microcrack growth

The model derivation in this subsection follows the formulation of Addessio and Johnson [1] and is here repeated for completeness of the proposed numerical model. Let us consider a penny-shaped crack shown in Fig. 1 with the unit normal vector **n**. Under conditions of normal traction, a crack grows when [25,10]:

$$F^{n'}(\sigma_{ij}, \bar{c}, n_i) = \sigma_{ij} n_j \sigma_{ik} n_k - \frac{1}{2} v_0 (\sigma_{ij} n_i n_j)^2 - \frac{K}{\bar{c}} \geqslant 0 \tag{15}$$

with

$$K \equiv \frac{\pi}{2} \frac{2 - v_0}{1 - v_0} \gamma G_0, \tag{16}$$

where v_0, G_0 and γ are the Poisson's ratio, shear modulus and crack surface energy, respectively, of the solid.

Similarly, a crack subjected to a shear is unstable when [10]

$$F^{t'}(\sigma_{ij}, \bar{c}, n_i) = (\sigma_t - \sigma_r)^2 - \frac{K}{\bar{c}} \geqslant 0, \tag{17}$$

where

$$\sigma_t = \sqrt{\sigma_{ij} n_j \sigma_{ik} n_k - (\sigma_{ij} n_i n_j)^2}, \tag{18}$$

$$\sigma_r = \sigma_0 - \mu_{\mathrm{f}} (\sigma_{ij} n_i n_j), \tag{19}$$

where σ_0 is the cohesive stress and μ_{f} is the coefficient of friction. For a given stress field σ_{ij}, Eqs. (15) and (17) provide a critical crack size. All cracks greater than or equal to the critical size grow. Cracks smaller than the critical size remain stable.

Continuum level representation of crack stability criteria is a damage surface and can be obtained through the following volume averaging procedure [1]:

$$\int_v \int_{\bar{c}} \int_{\Omega} F(\sigma_{ij}, \bar{c}, n_i) w(\bar{c}, \Omega) \, \mathrm{d}\bar{c} \, \mathrm{d}\Omega \, \mathrm{d}V \geqslant 0, \tag{20}$$

where w is the crack distribution function and Ω denotes orientations. Consider applying Eq. (20), with the assumptions of an exponential crack size distribution, to Eqs. (15) and (17). The resulting damage surface are defined in terms of the scalar parameters, p and q, defined as

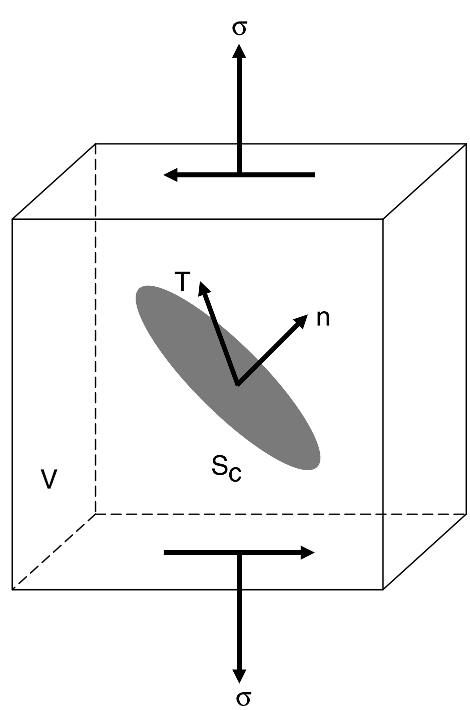

Fig. 1. Stresses on a crack (see also Fig. 1 of [1]).

$$p = -\frac{1}{3}\sigma_{ii}, \quad q = \sqrt{\frac{3}{2}q_{ij}q_{ij}}, \tag{21}$$

where p and q denote the pressure and the deviatoric stress norm, respectively. Two damage surfaces for tension and compression states were derived by Addessio and Johnson [1] using the averaging procedure in Eq. (20). In tension ($p < 0$),

$$F^n(p,q,\bar{c}) = q^2 + \frac{45}{4(5-v_0)}\left[(2-v_0)p^2 - \frac{2K}{\bar{c}}\right] = 0. \tag{22}$$

In compression ($p > 0$),

$$F^t(p,q,\bar{c}) = q^2 - \frac{45}{2(3-2v_0^2)}\left[(\mu_f p + \sigma_0)\left(\mu_f p + \sigma_0 + \sqrt{\frac{\pi K}{\bar{c}}}\right) + \frac{K}{\bar{c}}\right] = 0. \tag{23}$$

Fig. 2 is a graphical plot of damage surfaces for a carbon/polyurethane random fiber-reinforced composite in the $(p,q,\bar{c})$ space. The material properties and parameters of the carbon/polyurethane composite are $\kappa_0 = 213$ GPa, $\mu_0 = 187$ GPa, $\mu_f = 0.26$, $\gamma = 10$ Pa m, $\sigma_0 = 0$. Within the damage surfaces $[F(p,q,\bar{c}) \leqslant 0]$, the material is assumed to behave elastically and no microcracks grow (i.e. existing microcracks are arrested). Outside the damage surfaces $[F(p,q,\bar{c}) > 0]$, cracks grow until a state of stress that is within the surface is achieved.

The adopted formula for the rate of crack growth in the present study is [1]

$$\dot{\bar{c}} = \beta\dot{c}_{\max}\tanh(d_s) \tag{24}$$

with

$$d_s = q^2 - F_d \tag{25}$$

in which

$$\begin{aligned} F_d &= \frac{-45}{4(5-v_0)}\left[(2-v_0)p^2 - \frac{2K}{\bar{c}}\right], \quad p < 0 \\ &= \frac{45}{2(3-2v_0^2)}\left[(\mu_f p + \sigma_0)\left(\mu_f p + \sigma_0 + \sqrt{\frac{\pi K}{\bar{c}}}\right) + \frac{K}{\bar{c}}\right], \quad p > 0. \end{aligned} \tag{26}$$

In Eq. (24), $\dot{c}_{\max}$ is the shear wave speed $\left(\dot{c}_{\max} = \sqrt{\frac{E^*}{\rho^*}}\right)$, in which E^* and ρ^* are the effective Young's modulus and density, respectively, of the solid. In addition, d_s is the measure of the distance the amount by which the state of stress exceeds the damage surface, and β is the scaling factor for crack speed and is assumed to be constant.

According to the backward Euler method, the following approximations are made for the rate equation for crack growth:

$$\bar{c}_{n+1} = \bar{c}_n + \beta\Delta t_{n+1}\sqrt{\frac{(E^*)_{n+1}}{(\rho^*)_{n+1}}}\tanh(d_s), \tag{27}$$

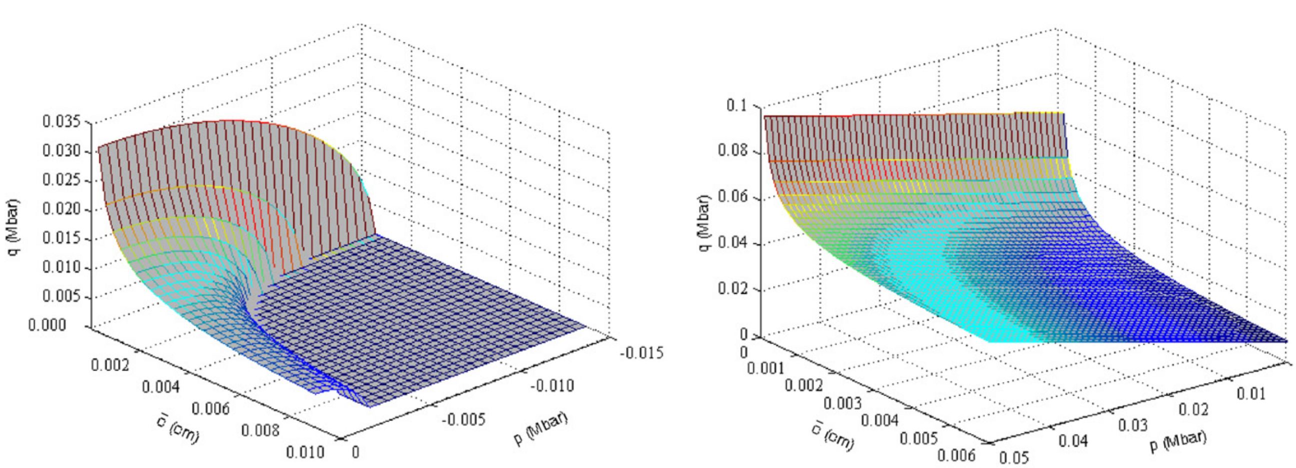

(a) Tensile ($p < 0$) damage surface

(b) Compressive ($p > 0$) damage surface

Fig. 2. A graphical plot of damage surfaces of carbon/polyurethane composites in the $(p,q,\bar{c})$ space.

where $\bar{c}_{n+1}$ can be evaluated by finding the root of the following scalar nonlinear equation at time $t = t_{n+1}$:

$$g(\bar{c}_{n+1}) = \bar{c}_{n+1} - \bar{c}_n - \beta \Delta t_{n+1} \sqrt{\frac{(E^*)_{n+1}}{(\rho^*)_{n+1}}} \tanh(d_s). \tag{28}$$

3. Effective moduli of microcracked brittle composites

Most studies in literature focused on the prediction of the effective moduli of microcracked materials are mainly the self-consistent method and differential scheme. The self-consistent analysis provided by [5] was focusing on randomly distributed, weakly interacting microcracks and provides the starting point for most analyses of microcracking in brittle materials. The self-consistent method was further explored by Hori and Nemat-Nasser [15], Laws et al. [32], Laws and Dvorak [31], Krajcinovic and Sumarac [28], Ju and Lee [20], etc. On the other hand, differential scheme has a long history. It was developed and used by Roscoe [41], and later extended by McLaughlin [34], Laws and Dvorak [31], and Hashin [13].

Clearly, it is imperative to construct a general model for the degradation of stiffness resulting from the nucleation and growth of microcracks in the brittle composites so that one can analyze the effects of density of microcracks in the composites. The overall stiffness tensor **C** in Eq. (8) of the microcracked brittle composite are estimated using the self-consistent method and differential scheme, and a completely general derivation of the self-consistent method and differential scheme for two different crack distributions is formulated in the present study.

3.1. Moduli of a brittle composite containing randomly distributed penny-shaped cracks

The normalized elastic moduli of a brittle composite containing randomly distributed penny-shaped cracks can be summarized as

Self-consistent estimates [5]:

$$\frac{E^*}{E_0} = 1 - \frac{16}{45} \frac{[1-(\nu^*)^2](10-3\nu^*)}{(2-\nu^*)} \omega, \tag{29}$$

$$\frac{G^*}{G_0} = 1 - \frac{32}{45} \frac{(1-\nu^*)(5-\nu^*)}{(2-\nu^*)} \omega, \tag{30}$$

$$\omega = \frac{45}{16} \frac{(\nu_0-\nu^*)(2-\nu^*)}{[1-(\nu^*)^2][10\nu_0 - \nu^*(1+3\nu_0)]}. \tag{31}$$

Differential scheme estimates [13]:

$$\frac{E^*}{E_0} = \left(\frac{\nu^*}{\nu_0}\right)^{10/9} \left(\frac{3-\nu_0}{3-\nu^*}\right)^{1/9}, \tag{32}$$

$$\frac{G^*}{G_0} = \frac{1+\nu_0}{1+\nu^*} \frac{E^*}{E_0}, \tag{33}$$

$$\omega = \frac{5}{8} \ln \frac{\nu_0}{\nu^*} + \frac{15}{64} \ln \frac{1-\nu^*}{1-\nu_0} + \frac{45}{128} \ln \frac{1+\nu^*}{1+\nu_0} + \frac{5}{128} \ln \frac{3-\nu^*}{3-\nu_0}, \tag{34}$$

where ν_0, E_0, G_0 are the Poisson's ratio, Young's modulus, and shear modulus, respectively, of an uncracked composite; and ν^*, E^*,G^* are the effective Poisson's ratio, Young's modulus, and shear modulus, respectively, of a cracked composite. $\omega = N\bar{c}^3$ signifies the crack density parameter. Accordingly, the initial crack density $\omega_0 = N_0\bar{c}^3$, where N_0 is the initial crack distribution per unit volume. The Newton iteration method is utilized to obtain the normalized elastic moduli E^*/E_0, G^*/G_0, and ν^*/ν_0.

3.2. Moduli of a brittle composite containing aligned penny-shaped cracks

The effective moduli of a brittle composite containing aligned penny-shaped cracks are formulated using the self-consistent method and differential scheme in this subsection.

3.2.1. Self-consistent estimates

Following Laws and Dvorak [31], the self-consistent estimates for the overall compliance of a cracked composite are defined as

$$\mathbf{M} = \mathbf{M}^0 + \frac{4\pi}{3}\omega\Lambda, \tag{35}$$

where $\mathbf{M}^0$ is the compliance of an uncracked composite. Note that the crack density parameter ω is not the same as the crack density parameter α introduced in Laws and Dvorak [31]. In the limit of aligned penny-shaped cracks, the material is transversely isotropic. The non-zero components of the tensor Λ for a transversely isotropic material are

$$\Lambda_{33} = \frac{2\gamma_1\gamma_2(\gamma_1+\gamma_2)}{\pi}\frac{M_{11}^2 - M_{12}^2}{M_{11}}, \tag{36}$$

$$\Lambda_{44} = \Lambda_{55} = \frac{4(\gamma_1+\gamma_2)(M_{11}^2 - M_{12}^2)(2M_{44})^{1/2}}{\pi[M_{11}(2M_{44})^{1/2} + (\gamma_1+\gamma_2)(M_{11}+M_{12})(M_{11}-M_{12})^{1/2}]}, \tag{37}$$

where γ_1^2 and γ_2^2 are the roots of

$$(M_{11}^2 - M_{12}^2)x^2 - [M_{11}M_{44} + 2M_{13}(M_{11} - M_{12})]x + M_{11}M_{33} - M_{13}^2 = 0. \tag{38}$$

Since the non-zero components of tensor Λ are Λ_{33} and Λ_{44} ($=\Lambda_{55}$), it follows:

$$M_{ij} = M_{ij}^0, \quad \text{if } M_{ij} \neq M_{33}, M_{44}, M_{55}. \tag{39}$$

Hence,

$$\Lambda_{33} = \frac{2\gamma_1\gamma_2(\gamma_1+\gamma_2)}{\pi}\frac{1-\nu_0^2}{E_0}, \tag{40}$$

$$\Lambda_{44} = \frac{4(\gamma_1+\gamma_2)(1-\nu_0^2)(2M_{44})^{1/2}}{\pi E_0[(2M_{44})^{1/2} + (\gamma_1+\gamma_2)(1-\nu_0)(1+\nu_0)^{1/2}E_0^{-1/2}]}, \tag{41}$$

where

$$\gamma_1\gamma_2 = \sqrt{\frac{E_0M_{33} - \nu_0^2}{1-\nu_0^2}}, \tag{42}$$

$$\gamma_1 + \gamma_2 = \sqrt{\frac{E_0M_{44} - 2\nu_0(1+\nu_0)}{1-\nu_0^2} + 2\sqrt{\frac{E_0M_{33} - \nu_0^2}{1-\nu_0^2}}}. \tag{43}$$

By combining Eqs. (35) and (40)–(43), we arrive at

$$M_{33} = \frac{1}{E_0} + \frac{8}{3}\omega\frac{1-\nu_0^2}{E_0}\sqrt{\frac{E_0M_{33} - \nu_0^2}{1-\nu_0^2}\left[\frac{E_0M_{44} - 2\nu_0(1+\nu_0)}{1-\nu_0^2} + 2\sqrt{\frac{E_0M_{33} - \nu_0^2}{1-\nu_0^2}}\right]}, \tag{44}$$

$$M_{44} = \frac{2(1+\nu_0)}{E_0} + \frac{16}{3}\omega\frac{1-\nu_0^2}{E_0}\frac{\sqrt{2M_{44}\left[\frac{E_0M_{44} - 2\nu_0(1+\nu_0)}{1-\nu_0^2} + 2\sqrt{\frac{E_0M_{33} - \nu_0^2}{1-\nu_0^2}}\right]}}{\sqrt{2M_{44}} + (1-\nu_0)\sqrt{\frac{(1+\nu_0)}{E_0}\left[\frac{E_0M_{44} - 2\nu_0(1+\nu_0)}{1-\nu_0^2} + 2\sqrt{\frac{E_0M_{33} - \nu_0^2}{1-\nu_0^2}}\right]}}. \tag{45}$$

Consequently, M_{33} and M_{44} can be evaluated by defining the following system of scalar nonlinear equations F_1^s and F_2^s:

$$F_1^s(M_{33}) = M_{33} - \frac{1}{E_0} - \frac{8}{3}\omega\frac{1-\nu_0^2}{E_0}\sqrt{\frac{E_0M_{33} - \nu_0^2}{1-\nu_0^2}\left[\frac{E_0M_{44} - 2\nu_0(1+\nu_0)}{1-\nu_0^2} + 2\sqrt{\frac{E_0M_{33} - \nu_0^2}{1-\nu_0^2}}\right]}, \tag{46}$$

$$F_2^s(M_{44}) = M_{44} - \frac{2(1+\nu_0)}{E_0} - \frac{16}{3}\omega\frac{1-\nu_0^2}{E_0}\frac{\sqrt{2M_{44}\left[\frac{E_0M_{44} - 2\nu_0(1+\nu_0)}{1-\nu_0^2} + 2\sqrt{\frac{E_0M_{33} - \nu_0^2}{1-\nu_0^2}}\right]}}{\sqrt{2M_{44}} + (1-\nu_0)\sqrt{\frac{(1+\nu_0)}{E_0}\left[\frac{E_0M_{44} - 2\nu_0(1+\nu_0)}{1-\nu_0^2} + 2\sqrt{\frac{E_0M_{33} - \nu_0^2}{1-\nu_0^2}}\right]}}, \tag{47}$$

where the roots M_{33} and M_{44} of the system of equations can be solved by a number of numerical methods. The Newton-iteration method can be used to obtain M_{33} and M_{44}.

3.2.2. Differential scheme estimates

Following Laws and Dvorak [31], the differential scheme estimates for the overall compliance of a brittle composite containing aligned penny-shaped cracks are obtained as

$$\frac{\mathrm{d}\mathbf{M}}{\mathrm{d}\omega} = \frac{4}{3}\pi\Lambda. \tag{48}$$

The only components of the compliance tensor $\mathbf{M}$ which are changed by the introduction of aligned penny-shaped cracks are M_{33}, M_{44}, and M_{55}, where $M_{44} = M_{55}$. Thus, the equations of the differential scheme model are

$$\frac{\mathrm{d}M_{33}}{\mathrm{d}\omega} = \frac{4}{3}\pi\Lambda_{33}, \tag{49}$$

$$\frac{\mathrm{d}M_{44}}{\mathrm{d}\omega} = \frac{4}{3}\pi\Lambda_{44}, \tag{50}$$

where Λ_{33} and Λ_{44} are given in Eqs. (40) and (41), respectively.

By substituting Eqs. (40) and (41) into Eqs. (49) and (50), we obtain the system of (first order) ordinary differential equations:

$$\frac{\mathrm{d}M_{33}}{\mathrm{d}\omega} = \frac{8}{3}\frac{1-v_0^2}{E_0}\sqrt{\frac{E_0M_{33}-v_0^2}{1-v_0^2}\left[\frac{E_0M_{44}-2v_0(1+v_0)}{1-v_0^2}+2\sqrt{\frac{E_0M_{33}-v_0^2}{1-v_0^2}}\right]} \equiv F_1^{\mathrm{d}}(\omega, M_{33}, M_{44}), \tag{51}$$

$$\frac{\mathrm{d}M_{44}}{\mathrm{d}\omega} = \frac{16}{3}\frac{1-v_0^2}{E_0}\frac{\sqrt{2M_{44}\left[\frac{E_0M_{44}-2v_0(1+v_0)}{1-v_0^2}+2\sqrt{\frac{E_0M_{33}-v_0^2}{1-v_0^2}}\right]}}{\sqrt{2M_{44}}+(1-v_0)\sqrt{\frac{(1+v_0)}{E_0}\left[\frac{E_0M_{44}-2v_0(1+v_0)}{1-v_0^2}+2\sqrt{\frac{E_0M_{33}-v_0^2}{1-v_0^2}}\right]}} \equiv F_2^{\mathrm{d}}(\omega, M_{33}, M_{44}) \tag{52}$$

with the initial conditions $M_{33}(0) = M_{33}^0 = \frac{1}{E_0}$ and $M_{44}(0) = M_{44}^0 = \frac{2(1+v_0)}{E_0}$.

We now turn to the problem of dealing with the system of ordinary differential equations. Since the differential equations in Eqs. (51) and (52) cannot be solved analytically, we resort to the numerical solution. The system of ordinary differential equations in Eqs. (51) and (52) can be rephrased as a basic problem (replacing the subscripts 33 and 44 with 1 and 2, respectively):

$$\frac{\mathrm{d}M_i}{\mathrm{d}\omega} = F_i^{\mathrm{d}}(\omega, M_1, M_2), \quad i = 1,2 \tag{53}$$

subject to the initial conditions

$$M_i(0) = M_i^0, \quad i = 1,2. \tag{54}$$

The Runge–Kutta method is used to solve the basic problem (53).

Finally, the stiffness matrix of the brittle composite containing aligned penny-shaped cracks can be obtained by replacing the components M_{33}^0 and M_{44}^0 with the roots M_{33} and M_{44} of Eqs. (46) and (47) or Eqs. (51) and (52), in conjunction with the inverse of generalized Hook's law. The final expression takes the form

$$\mathbf{C} = E_0\begin{bmatrix} \frac{-E_0M_{33}+v_0^2}{(1+v_0)[E_0M_{33}(v_0-1)+2v_0^2]} & -\frac{v_0(E_0M_{33}+v_0)}{(1+v_0)[E_0M_{33}(v_0-1)+2v_0^2]} & -\frac{v_0}{E_0M_{33}(v_0-1)+2v_0^2} & 0 & 0 & 0 \\ -\frac{v_0(E_0M_{33}+v_0)}{(1+v_0)[E_0M_{33}(v_0-1)+2v_0^2]} & \frac{-E_0M_{33}+v_0^2}{(1+v_0)[E_0M_{33}(v_0-1)+2v_0^2]} & -\frac{v_0}{E_0M_{33}(v_0-1)+2v_0^2} & 0 & 0 & 0 \\ -\frac{v_0}{E_0M_{33}(v_0-1)+2v_0^2} & -\frac{v_0}{E_0M_{33}(v_0-1)+2v_0^2} & \frac{v_0-1}{E_0M_{33}(v_0-1)+2v_0^2} & 0 & 0 & 0 \\ 0 & 0 & 0 & \frac{1}{E_0M_{44}} & 0 & 0 \\ 0 & 0 & 0 & 0 & \frac{1}{E_0M_{44}} & 0 \\ 0 & 0 & 0 & 0 & 0 & \frac{1}{2(1+v_0)} \end{bmatrix}. \tag{55}$$

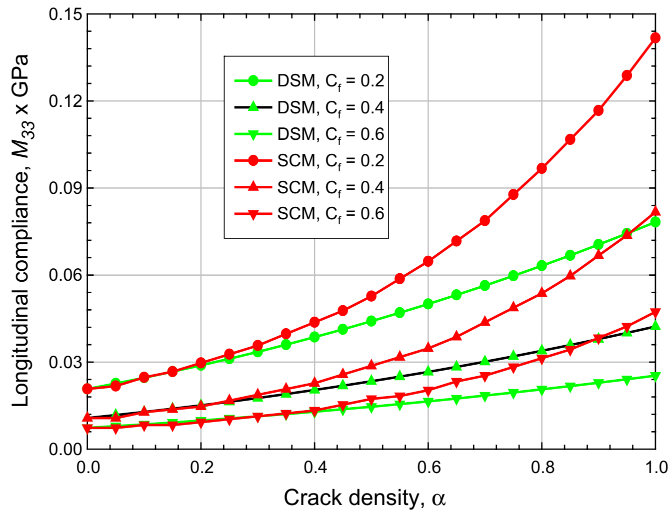

Fig. 3. The comparison of longitudinal compliance M_{33} predicted by self-consistent method and differential scheme (see also Fig. 1 of [31]).

The stiffness matrix in Eq. (55) shows that the brittle composite containing aligned penny-shaped cracks is transversely isotropic.

Predictions of longitudinal compliance M_{33} of a random fiber-reinforced composite with aligned penny-shaped cracks using the two methods, self-consistent method and differential scheme, are shown in Fig. 3 to exhibit the difference of the nature of two different formulations. Data for the uncracked composite with volume fractions $c_f = 0.2, 0.4, 0.6$ are taken from Table 2 of Dvorak et al. [11]. It is noted that the longitudinal compliance M_{33} obtained by differential scheme is lower than that by self-consistent method.

4. Numerical simulations

The proposed constitutive model is implemented into the FE codes DYNA3D and ABAQUS to predict the constitutive behavior and crack evolution in brittle composites. The constitutive model is portable to both commercial (ABAQUS) and publicly available (DYNA3D) FE codes. Iterative computational algorithms accounting for the crack nucleation and growth in brittle composites explained in Fig. 2(b) and (c) of Lee et al. [33] are utilized to combine damage mechanisms into the constitutive relation. The implemented computational model is then applied to through a benchmark problem, one (finite) element test on random, fiber-reinforced composites, to illustrate the characteristics of the model.

The one-element test is commonly used as a benchmark for determining the global characteristics of a material model. The schematics of the test can be found in Lee et al. [33]. The ratio of thickness, width, and length of the composite specimen is 1:10:100. The prescribed velocity $v(t)$ imposed on the top of the specimen is related to the rate of strain as follows:

$$v(t) = \dot{\epsilon}L = \dot{\epsilon}L_0 \cdot \exp(\dot{\epsilon}t), \tag{56}$$

where L_0 and L denote the heights of the original and deformed specimens, respectively. The material properties of the composite used in this simulation are: $\rho = 3177\ \mathrm{kg/m^3}$, $\kappa = 213$ GPa, $\mu = 187$ GPa, $\gamma = 10.0$ Pa m, $\sigma_{n0} = 1.0 \times 10^{10}\ \mathrm{N/m^2}$, $\dot{N}_0 = 1.0 \times 10^{11}/\mathrm{s/m^3}$, and $\sigma_1 = 2.0 \times 10^9\ \mathrm{N/m^2}$. These values are chosen from a combination of experimental results from the literature and do not correspond to a specific composite.

To illustrate the crack evolution and strain softening behavior of the composite, the predicted stress–strain curve and corresponding evolutions of the number of cracks per unit volume and the mean crack size are shown in Figs. 4 and 5, respectively. It is observed from Fig. 5 that the number of cracks per unit volume remains constant within the initial stage of loading, begins to increase rapidly at the lower threshold value of strain up to the upper threshold value of strain, and then remains constant again even at the deep strain range, while the mean crack size remains constant up to the threshold strain but, after that point, it suddenly begins to increase until the compressed specimen reaches its ultimate strength. It is concluded from this numerical simulation that the crack growth mechanism mainly influences the softening behavior of the brittle composites.

The effects of strain rate of applied loading on the crack evolution and constitutive behavior of the composite are analyzed. The predicted stress–strain curves and corresponding evolutions of the crack size as a function of the uniaxial strain with strain rates of 0.1/s, 20/s, 50/s are shown in Figs. 6 and 7, respectively. It is seen from Fig. 6 that the strain rate affects the onset point of the nonlinear stress–strain curve and the maximum stress the material can sustain, and controls the rate of crack growth. In Fig. 7, it is observed that cracks grow more rapidly as the strain rate decreases.

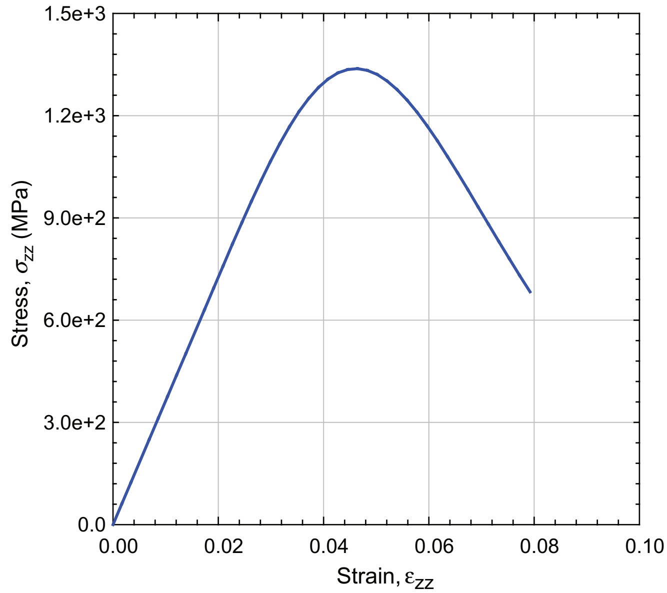

Fig. 4. The predicted stress–strain curve, showing strain softening behavior after the peak load.

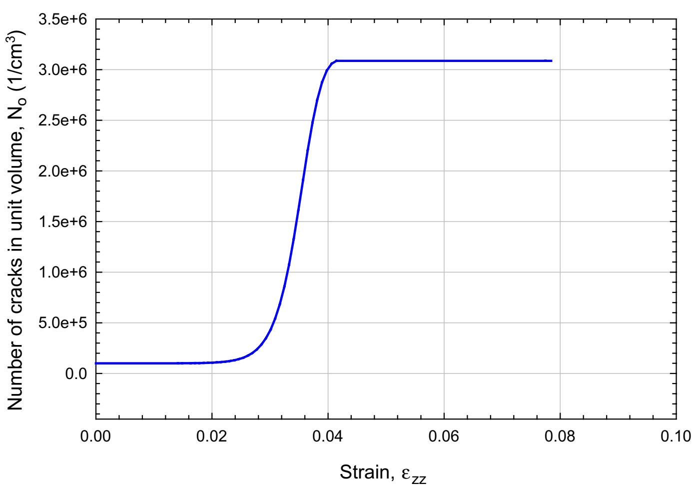

(a) Crack nucleation

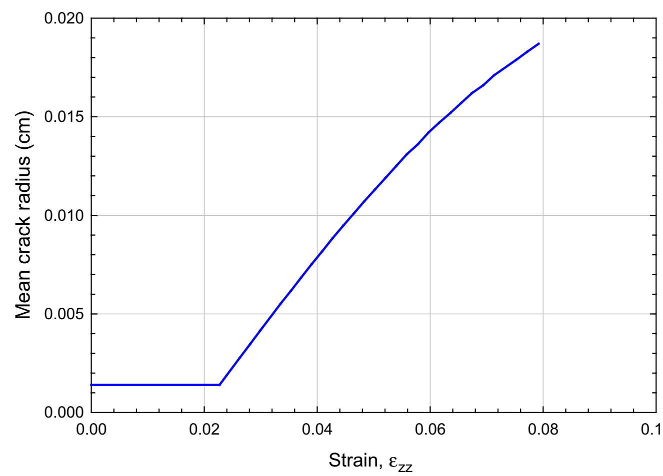

(b) Crack growth

Fig. 5. The predicted evolutions of the number of cracks per unit volume (a) and mean crack size (b) versus strain corresponding to Fig. 4.

5. Experimental comparison

To verify the present framework, the present predictions are compared with some available experimental data. First, we compare the present prediction with experimental data provided by Meraghni and Benzeggagh [36] for three-dimensional random, fiber-reinforced composites. Here, we adopt the material properties according to Meraghni and Benzeggagh [36] as follows: $\kappa = 14.02$ GPa, $\mu = 6.28$ GPa, $\rho = 1403$ kg/m^3.

Using the parameter estimation algorithm developed by Simo et al. [47], we estimate the crack nucleation and growth parameters to be $\dot{N}_0 = 1.5 \times 10^{14}/\text{s/m}^3$, $\sigma_{n0} = 0.5 \times 10^7$ N/m^2, $\sigma_1 = 1.0 \times 10^7$ N/m^2; $\bar{c} = 0.1 \times 10^{-4}$, $N_0 = 1.0 \times 10^{11}/\text{m}^3$, $\mu_f = 0.26$, $\gamma = 10.0$ Pa m, $\beta = 0.5 \times 10^{-5}$. Based on the above material properties and parameters, we depict the present prediction against three experimental data provided by Meraghni and Benzeggagh [36] in Fig. 8. It is observed from the figure that the stress–strain curve for the present prediction is well within the experimentally obtained curves. Fig. 9 exhibits the evolution of the number of cracks per unit volume versus uniaxial strain corresponding to Fig. 8. As the strain increases, the present prediction exhibits nonlinear response even in early stage due to crack nucleation as shown in Fig. 8. Fig. 10 exhibits the normalized effective Young's modulus as a function of the crack density. Since we assume the two damage processes, crack nucleation and crack growth, to be occurred sequentially and independently, only the crack nucleation

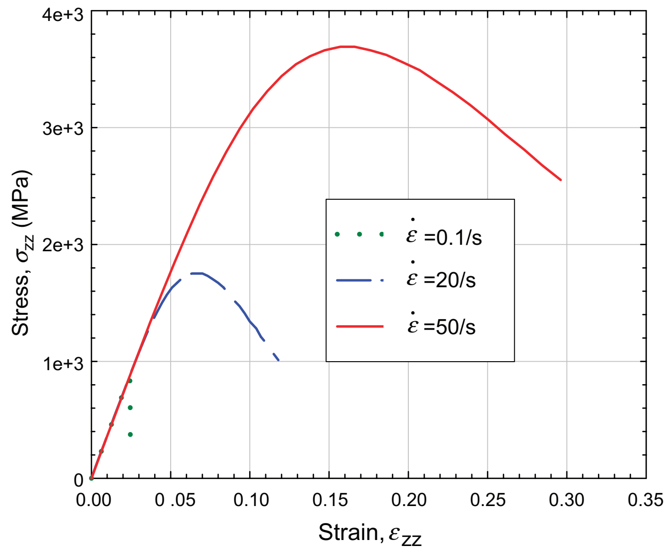

Fig. 6. The present predicted stress–strain curves for strain rates of $\dot{\varepsilon} = 0.1$/s, 20/s, 50/s.

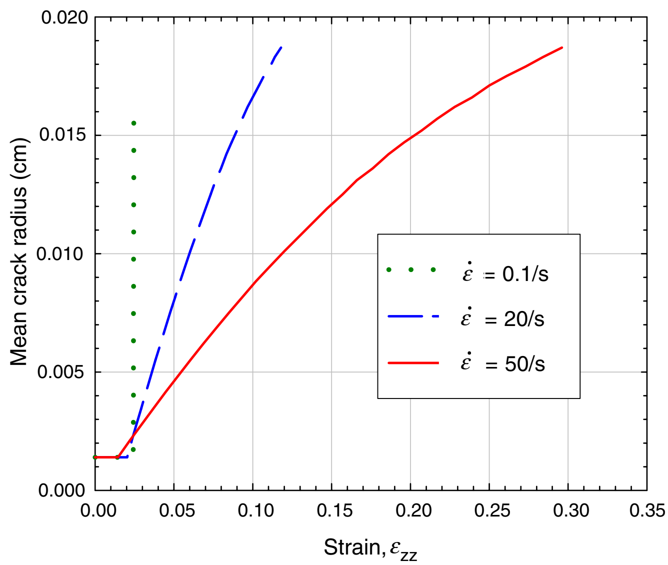

Fig. 7. The predicted evolutions of mean crack size versus strain for strain rates of $\dot{\varepsilon} = 0.1$/s, 20/s, 50/s corresponding to Fig. 6.

is modeled as an active damage mechanism within the small strain range. Accordingly, the normalized effective Young's modulus from the present prediction is shown to be slightly higher than that based on the experiment in the figure.

We further compare the present prediction with experimental data on brittle ceramic matrix composites reported by Stawovy et al. [48] to further convince the predictive capability of the proposed model. The same material properties for the m-cordierite ceramic matrix composites are employed in this simulation according to Stawovy et al. [48] as follows: $E_{\mathrm{m}} = 130$ GPa, $\phi_{\mathrm{m}} = 0.6$; $E_{\mathrm{f}} = 200$ GPa, $\phi_{\mathrm{f}} = 0.4$, where the subscripts m and f denote the matrix and fibers, respectively. The overall Young's modulus of the composites is estimated simply by a rule of mixtures as follows: $E = E_{\mathrm{m}}\phi_{\mathrm{m}} + E_{\mathrm{f}}\phi_{\mathrm{f}} = 158$ GPa. The typical values of Poisson's ratio and density of the ceramic matrix composites ($\nu = 0.24$, $\rho = 2100$ kg/m^3) are used in this simulation. Parameter estimation procedures [47] adopted from the above experimental comparison are not applicable to this experimental comparison due to the lack of experimental data reported by Stawovy et al. [48]. Instead, the crack nucleation and growth parameters are estimated using the trial-and-error method to be $\dot{N}_0 = 1.5 \times 10^{14}$/s/m^3, $\sigma_{n0} = 0.5 \times 10^7$ N/m^2, $\sigma_1 = 1.0 \times 10^7$ N/m^2; $\bar{c} = 0.1 \times 10^{-4}$, $N_0 = 1.45 \times 10^{14}$/m^3, $\mu_{\mathrm{f}} = 0.26$, $\gamma = 0.8$ Pa m, $\beta = 0.1 \times 10^{-6}$. Based on the above material properties and parameters, we depict the present prediction against experimental data provided by Stawovy et al. [48] in Fig. 11. We observe from the figure that the stress–strain curve

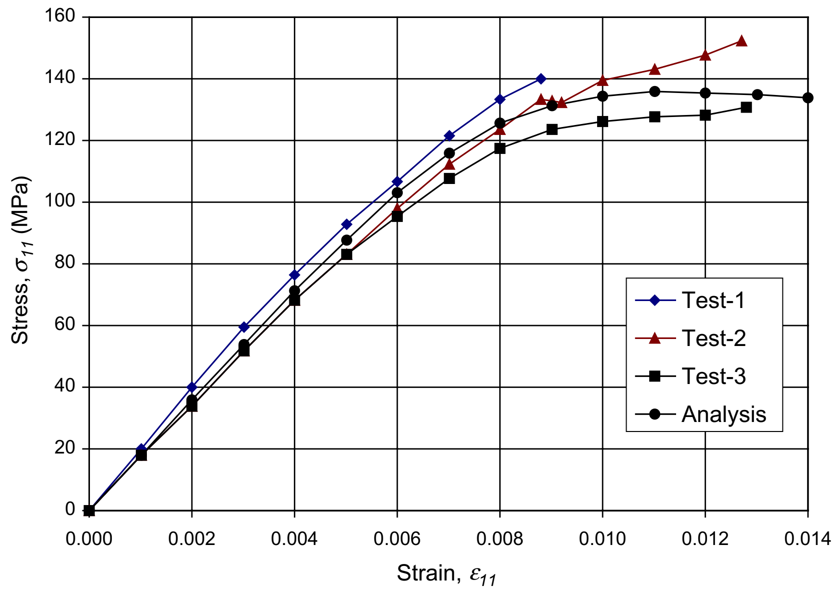

Fig. 8. The comparison between the present prediction and experimental data [36] for overall uniaxial tensile responses of three-dimensional random fiber composites.

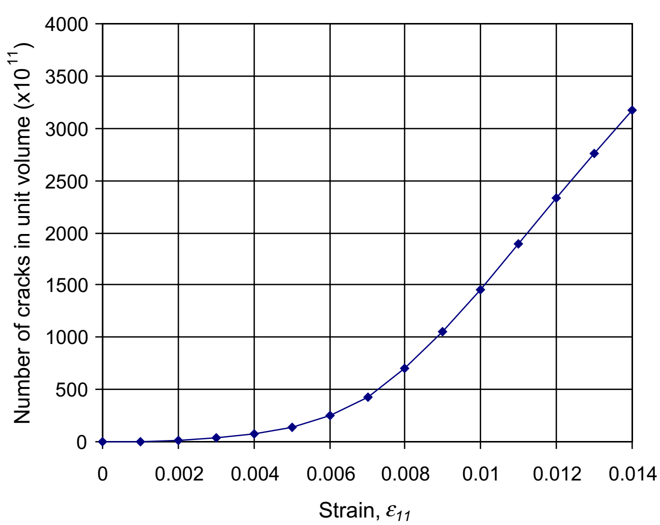

Fig. 9. Evolutionary history of crack nucleation versus strain corresponding to Fig. 8.

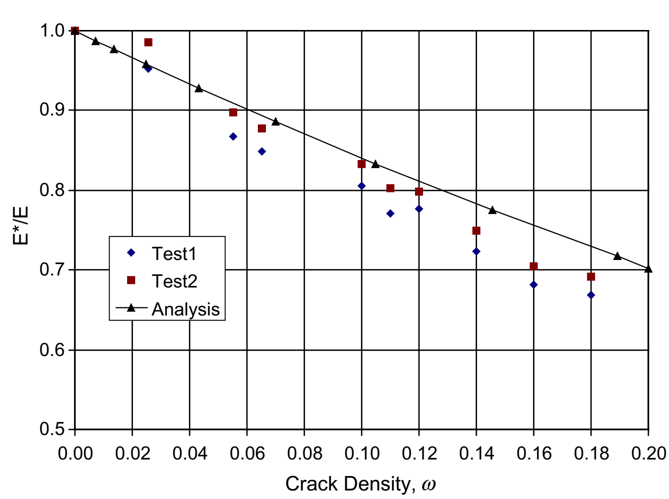

Fig. 10. The comparison of normalized overall Young's modulus versus crack density between the present prediction and experimental data [36].

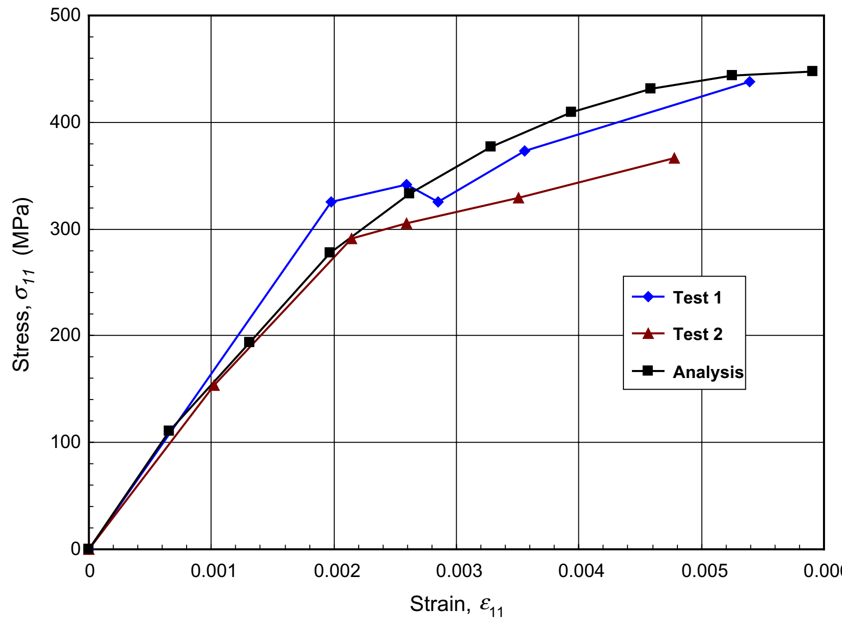

Fig. 11. The comparison between the present prediction and experimental data [48] for overall uniaxial tensile responses of ceramic matrix composites.

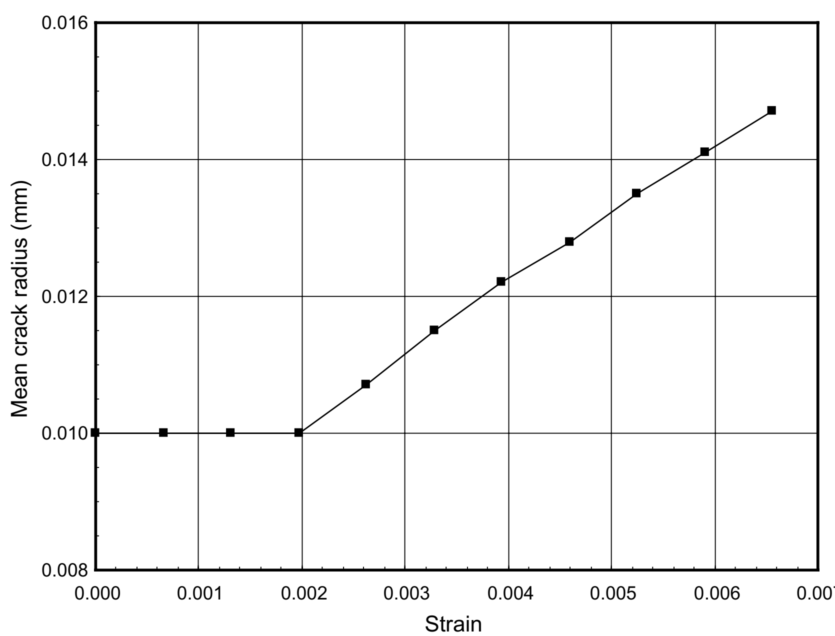

Fig. 12. Evolutionary history of crack size versus strain corresponding to Fig. 11.

for the present prediction is well within the two experimental data. It is also found during this simulation that the effect of microcrack nucleation on the stress–strain response of the composites is negligible and microcracks start to grow even in early stage during the uniaxial tension. The evolution of the crack size versus strain is plotted in Fig. 12. Fig. 13 shows the sequence of deformed shape and von Mises effective stress of the composite specimen during the uniaxial tension.

6. Concluding remarks

A constitutive model was developed based on a combination of a fracture-mechanics based model and micromechanical formulations for simulation of the effective mechanical properties and crack evolution in damage-tolerant brittle composites. The fracture-mechanics based model employed Seaman et al. [45] and Addessio and Johnson's [1] rate equations for

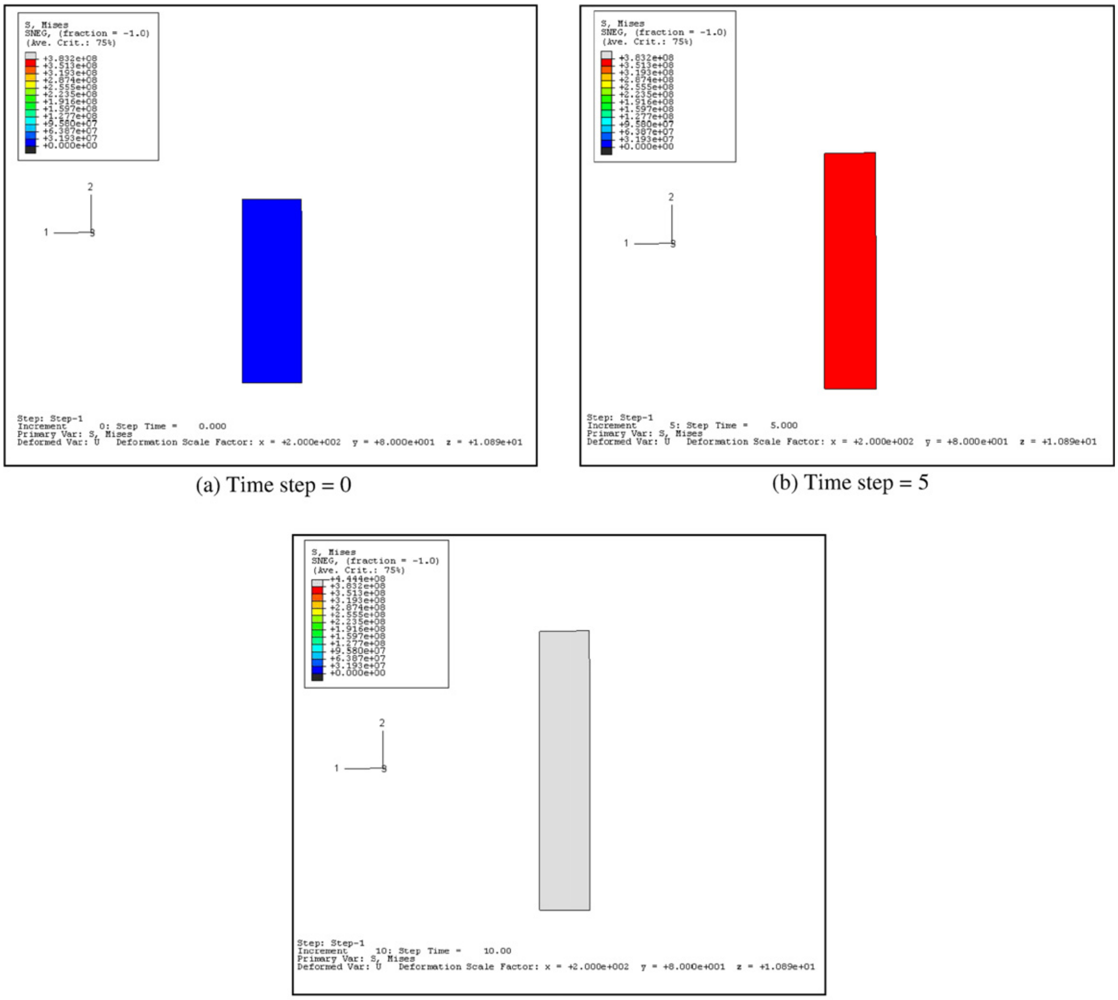

(a) Time step = 0

(b) Time step = 5

(c) Time step = 10

Fig. 13. The sequence of deformed shape and von Mises effective stress during the uniaxial tension.

evolving microstructure. Effective mechanical properties of microcracked brittle composites containing different crack distributions were modeled using the self-consistent method and differential scheme. The Newton-iteration method were used to estimate the effective moduli of the composites.

The constitutive model was implemented into the finite element codes DYNA3D and ABAQUS to simulate the constitutive behavior and crack evolution of brittle composites. The capability of the present computational damage approaches to model progressive deterioration of effective stiffness, crack evolution and softening behavior of the damage tolerant brittle composites was shown systematically from the benchmark one-element numerical test on the coupon under compression and tension. The effects of strain rate of applied loading on the crack evolution and constitutive behavior of the composites were also analyzed from the benchmark test. Finally, to verify the present framework, we compared the present predictions with experimental data provided by Meraghni and Benzeggagh [36] and Stawovy et al. [48] for three-dimensional brittle composites. The good agreement between the present prediction and experiments is encouraging for possible use of the proposed methodology to predict the effective mechanical properties and crack evolution in damage-tolerant brittle composites.

However, investigations on determining the model parameters and further simulations of the brittle composites under loading paths other than a uniaxial loading (e.g., shear, multi-axial state, cyclic loading, etc.) are needed to realistically assess the performance of the proposed computational model and methodology.

Acknowledgments

This research was sponsored by (1) the US Department of Energy, Assistant Secretary for Energy Efficiency and Renewable Energy, Office of Transportation Technologies, Lightweight Materials Program, under contract DE-AC05-00OR22725 with UT-Battelle, LLC; and (2) the Ministry of Science and Technology, Korea, for the financial support by a grant (NC33676, R11-2002-101-02004-0) from the Smart Infra-Structure Technology Center (SISTeC), Korea. The authors would like to thank the reviewer for his/her elaborated comments on the original manuscript. The first author would also like to thank Dr. D.K. Shin (Myongji University), and Mr. B.R. Kim and Mr. S.K. Ha (KAIST) for conducting the relevant simulations.

References

[1] F.L. Addessio, J.N. Johnson, A constitutive model for the dynamic response of brittle materials, J. Appl. Phys. 67 (1990) 3275–3286.
[2] P.F. Arndt, T. Nattermann, Criterion for crack formation in disordered materials, Phys. Rev. B (Condens. Matter Mater. Phys.) 63 (2001) 134204/1–8.
[3] T.W. Barbee, L. Seaman, R.C. Crewdson, Dynamic fracture criteria of homogeneous materials, AFWL-TR-70-99, Air Force Weapons Laboratory, Albuquerque, NM, 1970.
[4] Z. Bazant, Fracture and Size Effect in Concrete and Other Quasi-brittle Materials, CRC Press, 1998.
[5] B. Budiansky, R.J. O'Connell, Elastic moduli of a cracked solid, Int. J. Solids Struct. 12 (1976) 81–97.
[6] G.T. Camacho, M. Ortiz, Computational modelling of impact damage in brittle materials, Int. J. Solids Struct. 33 (1996) 2899–2938.
[7] B.K. Chakrabarti, L.G. Benguigui, Statistical Physics of Fracture and Breakdown in Disordered Systems, Clarendon Press, 1997.
[8] D.R. Curran, D.A. Shockey, L. Seaman, Dynamic fracture criteria for a polycarbonate, J. Appl. Phys. 44 (1973) 4025–4038.
[9] A. Delaplace, G. Pijaudier-Cabot, S. Roux, Progressive damage in discrete models and consequences on continuum modelling, J. Mech. Phys. Solids 44 (1996) 99–136.
[10] J.K. Dienes, Statistical crack mechanics, in: Proceedings of the Collogue International du CNRS no. 351, France, 1983.
[11] G.J. Dvorak, N. Laws, M. Hejazi, Analysis of progressive matrix cracking in composite laminates. I. Thermoelastic properties of a ply with cracks, J. Compos. Mater. 19 (1985) 216–234.
[12] A. Hansen, S. Roux, Statistical toolbox for damage and fracture, in: D. Krajcinovic, van Mier (Eds.), Damage and Fracture of Disordered Materials, Springer, 2000, pp. 17–101.
[13] Z. Hashin, The differential scheme and its application to cracked materials, J. Mech. Phys. Solids 36 (1988) 719–734.
[14] H.J. Herrmann, S. Roux, Statistical Models for the Fracture of Disordered Media, North-Holland, 1990.
[15] H. Hori, S. Nemat-Nasser, Overall moduli of solids with microcracks: load-induced anisotropy, J. Mech. Phys. Solids 31 (1983) 155–171.
[16] H. Horii, A. Hasegawa, F. Nishino, Fracture process and bridging zone model and influencing factors in fracture of concrete, in: S.P. Shah, S.E. Swartz (Eds.), Fracture of Concrete and Rock, Springer-Verlag, New York, 1989, pp. 205–219.
[17] M.B. Isichenko, Percolation, statistical topography, and transport in random media, Rev. Modern Phys. 64 (1992) 961–1043.
[18] A. Jagota, S.J. Bennison, Element breaking rules in computational models for brittle fracture, Modell. Simulat. Mater. Sci. Engrg. 3 (1995) 485–501.
[19] M. Jirasek, Comparative study on finite elements with embedded discontinuities, Comput. Methods Appl. Mech. Engrg. 188 (2000) 307–330.
[20] J.W. Ju, X. Lee, On three-dimensional self-consistent micromechanical damage models for brittle solids, Int. J. Solids Struct. 27 (1991) 227–258.
[21] M. Kachanov, Effective elastic properties of cracked solids: critical review of some basic concepts, Appl. Mech. Rev. 45 (1992) 304–334.
[22] M. Kachanov, Elastic solids with many cracks and related problems, Adv. Appl. Mech. 30 (1994) 259–445.
[23] B.L. Karihaloo, D. Fu, X. Huang, Modeling of tension softening in quasi-brittle materials by an array of circular holes with edge cracks, Mech. Mater. 11 (1991) 123–134.
[24] B.L. Karihaloo, X. Huang, Tensile response of quasi-brittle, PAGEOPH 137 (1991) 461–487.
[25] L.M. Keer, A note on shear and combined loading for a penny-shaped crack, J. Mech. Phys. Solids 14 (1966) 1–6.
[26] D. Krajcinovic, Damage Mechanics, Elsevier, 1996.
[27] D. Krajcinovic, J. van Mier, Damage and Fracture of Disordered Materials, Springer, Series: ISM International Centre for Mechanical Sciences, NR. 410, 2000.
[28] D. Krajcinovic, D. Sumarac, A mesomechanical model for brittle deformation process. Part I, J. Appl. Mech. 56 (1989) 51–62.
[29] D. Krajcinovic, M. Vujosevic, Intrinsic failure modes of brittle materials, Int. J. Solids Struct. 35 (1998) 2487–2503.
[30] B. Lawn, Fracture of Brittle Solids, Cambridge Solid State Science Series, Cambridge University Press, 1993.
[31] N. Laws, G.J. Dvorak, The effect of fiber breaks and aligned penny-shaped cracks on the stiffness and energy release rates in unidirectional composites, Int. J. Solids Struct. 23 (1987) 1269–1283.
[32] N. Laws, G.J. Dvorak, M. Hejazi, Stiffness changes in unidirectional composites caused by crack systems, Mech. Mater. 2 (1983) 123–137.
[33] H.K. Lee, S. Simunovic, D.K. Shin, A computational approach for prediction of the damage evolution and crushing behavior of chopped random fiber composites, Comput. Mater. Sci. 29 (2004) 459–474.
[34] R. McLaughlin, A study of the differential scheme for composite materials, Int. J. Engrg. Sci. 15 (1977) 237–244.
[35] P. Meakin, Models for material failure and deformation, Science 252 (1991) 226–234.
[36] F. Meraghni, M.L. Benzeggagh, Micromechanical modeling of matrix degradation in randomly discontinuous-fibre composites, Compos. Sci. Technol. 55 (1995) 171–186.
[37] L.L. Mishnaevsky, Methods of the theory of complex systems in modelling of fracture: a brief review, Engrg. Fract. Mech. 56 (1997) 47–56.
[38] J. Oliver, A.E. Huespe, M.D.G. Pulido, E. Chaves, From continuum mechanics to fracture mechanics: the strong discontinuity approach, Engrg. Fract. Mech. 69 (2002) 113–136.
[39] M. Ortiz, Microcrack coalescence and macroscopic crack growth initiation in brittle solids, Int. J. Solids Struct. 24 (1988) 231–250.
[40] M. Ortiz, Y. Leroy, A. Needleman, A finite element method for localized failure analysis, Comput. Methods Appl. Mech. Engrg. 61 (1987) 189–214.
[41] R. Roscoe, The viscosity of suspensions of rigid spheres, Brit. J. Appl. Phys. 3 (1952) 267–269.
[42] M. Sahimi, Non-linear and non-local transport processes in heterogeneous media: from long-range correlated percolation to fracture and materials breakdown, Phys. Rep. 306 (1998) 213–395.
[43] E. Schlangen, E.J. Garboczi, Fracture simulations of concrete using lattice models: computational aspects, Engrg. Fract. Mech. 57 (1997) 319–332.
[44] L. Seaman, T.W. Barbee, D.R. Curran, Dynamic fracture criteria of homogeneous materials, AFWL-TR-71-156, Air Force Weapons Laboratory, Albuquerque, NM, 1971.
[45] L. Seaman, D.R. Curran, D.A. Shockey, Computational models for ductile and brittle fracture, J. Appl. Phys. 47 (1976) 4814–4826.

[46] D.A. Shockey, L. Seaman, D.R. Curran, Dynamic fracture of beryllium under plate impact and correlation with electron beam and underground test results, AFWL-TR-73-12, Air Force Weapons Lab., Albuquerque, NM, 1973.
[47] J.C. Simo, J.W. Ju, K.S. Pister, R.L. Taylor, Assessment of Cap Model: consistent return algorithm and rate-dependent extension, J. Engrg. Mech. 114 (1988) 191–218.
[48] R.H. Stawovy, S.L. Kampe, W.A. Curtin, Mechanical behavior of glass and blackglass ceramic matrix composites, Acta Mater. 45 (1997) 5317–5325.
[49] S. Straumsnes, P. Dommersnes, E.G. Flekkoy, S. Roux, Damage due to self-similar micro-cracking, Euro. J. Mech. A/Solids 16 (1997) 993–1009.